International Journal of Science and Research (IJSR)
ISSN (Online): 2319-7064
Index Copernicus Value (2013): 6.14 | Impact Factor (2015): 6.391

Vibrational Spectra and Structural Properties of 2,2,6,6-Tetramethyl Piperidone by Density Functional Theory

G. Mahalakshmi[1], K. Revathi[2], V. Balachandran[3]

[1, 2]Research Department of Physics, Government Arts College (Autonomou), Karur-639 001, India

[3]Research Department of Physics, A A Government Arts College, Musiri 621 211, India

Abstract: ***Vibrational intensities are both experimentally measured and theoretically important physical quantities which are directly related to the distribution of the electric charges in a molecule. In this paper, the molecule TMP(2,2,6,6-tetramethyl piperidone) have been studied extensively utilizing ab initio Hartee-fock(HF) and density functional frequencies are calculated and scaled values were compared with experimental values. The study of the assignment is performed on the basis of total energy distribution (TED). FT-IR and FT-Raman spectra of TMP have been recorded. IR, Raman intensities, HOMO-LUMO, NBO analysis were investigated. The electric dipole moment, polarizability and first hyper polarizability of the molecule is computed. The UV absorption spectrum of the title molecule that dissolved in solvents were examined in the range of 200-400 nm.***

Keywords: DFT, 2,2,6,6-tetramethyl piperidone, HOMO-LUMO, NBO, hyperpolarisability

1. Introduction

Piperidone and its derivatives are widely used in the pharmacological industry due to their biological activities. The actual pharmacological activity of the compound is determined by the nature, size and the position of the side groups attached to the ring. Piperidone derivatives have many medical properties such as anti-hypoxic, anti-mycotic, psycotropic activities. Some of these derivatives also have herbicidal, bactericidal and mutagenetic activities [1]. The amino ketones like 2,6-diphenyl piperidones and their substituted compounds have been studied by the researchers in recent years due to the potent analgesic character [2]. These are most often synthesised by means of the addition of a primary amine to 2 moles of an alkyl acrylate followed by the dieckmann condensation hydrolysis and decarboxylation [3]. A classic named reaction for the synthesis of piperidones is the Petrenko – Kritschenko Piperidone synthesis which involves combining an alkyl -1, 3 – acetonedicarboxylate with benzaldehyde and amine. This multi component reaction is related to the Hantzsch pyridine synthesis [4]. Its proven application in wittig reaction with Phosphorus Ylides, Organic Photoreceptor Synthesis, Removal of sulphur compounds from gases, Pethidine Synthesis, Pharmaceutical Synthesis, Synthesis of Spyro - Heterocycles and Fused ring Systems [5]

Many theoretical studies proved the importance of the molecule due to its various applications. Further these crystalline compounds have ring structures and several functional groups. The study of intermolecular interaction, vibrations and forces between the atoms in the molecules are very much useful for the better understanding of the title compounds. Consideration of these factors led to undertake detailed spectral investigation of 2,2,6,6-tetramethyl piperidone (TMP) through FT-IR and FT-RAMAN which shows the structure and specification of this compound.

2. Experimental Details

The title compound 2,2,6,6 - tetramethyl piperidone (TMP) is obtained from Sigma Aldrich chemical company, England and used as such to record FT-IR and FT-Raman spectra. The FT-IR spectrum of TMP was recorded in the region 4000 – 500 cm^{-1} using KBr pellet. The Bruker IFS 66V model FT-IR spectrometer was used for the spectral measurements. The global and mercury arc sources, KBr beam splitters are used while recording FT-IR spectra of the title compound TMP. The FT-Raman spectrum was recorded on a Bruker IFS-66V model interferometer equipped with an FRA-106 FT-Raman accessory. The spectrum was recorded in the region (4000 – 0 cm^{-1}) using the nm line of an Nd: YAG laser for excitation operating at 200 mw of power.

Computational Methods

Quantum chemical calculations were carried out by means of the Gaussian 09w program package [6] with Becke3-Lee-Yang-Parr (B3LYP) DFT/HF functional with standard 6-311++G(d,p) basis set [7,8]. The Cartesian representation of the theoretical force constants had been computed at the optimized geometry by assuming C_1 point group symmetry. The comparison between the calculated and the observed vibrational spectra helps us to understand the observed spectral features. In order to improve the agreement of theoretically calculated frequencies with experimentally calculated frequencies, it is necessary to scale down the theoretically calculated harmonic frequencies. Hence, the vibrational frequencies theoretically calculated at HF and B3LYP/6-311++G(d,p) are scaled down by using MOLVIB 7.0 version written by Sundius [9,10].

The first hyperpolarizability and the chemical shift of the atoms of TMP have been calculated using B3LYP/6-311++G(d,p) method. The HOMO–LUMO analysis has been carried out to explain the charge transfer within the compound. The chemical hardness (η) and chemical

Licensed Under Creative Commons Attribution CC BY

potential (μ) have been calculated using the highest occupied molecular orbital (HOMO) and lowest unoccupied molecular orbital (LUMO). NBO analysis has been performed on TMP using B3LYP/6-311++G (d,p) level in order to elucidate the intermolecular hydrogen bonding, intermolecular charge transfer (ICT), rehybridization, delocalization of electron density.

Prediction of Raman Intensities and Hyperpolarisaility

The Raman activities (S_i) calculated with the help of GAUSSIAN 09 program are converted to relative Raman intensities (I_i) using the following relationship derived from the basic theory of Raman scattering [11, 12].

$$I_i = \frac{f(v_0 - v_i)^4 s_i}{v_i\left[1 - \exp\left(\frac{-hcv_i}{k_b T}\right)\right]}$$

In the above formula ν_o is the laser exciting frequency in cm^{-1} (in this work, we have used the excitation wave number ν_0 = 9398.5 cm^{-1}, which corresponds to the wavelength of 1064 nm of a Nd :YAG laser), ν_i is the vibrational wave number of the i^{th} normal mode (cm^{-1}) and S_i is the Raman scattering activity of the normal mode ν_i. f (is the constant equal to 10^{-12}) is the suitably chosen common normalization factor for all peak intensities. h ,k, c and T are Planck's constant, Boltzmann constant, speed of light and temperature in Kelvin, respectively

3. Results and Discussion

Optimized Geometry

The optimized molecular structure of TMP is shown in Fig. 1 which was calculated using Gaussian 09w program. The calculated optimized geometrical parameters of the title compound are presented in Table 1. The bond lengths and bond angles are determined from the geometrical parameters obtained from HF and DFT method. The optimized structure can be compared with other similar systems for which the crystal structures have been solved. Therefore optimized geometrical parameters of TMP are compared with the experimental data of similar kind of molecules [13].

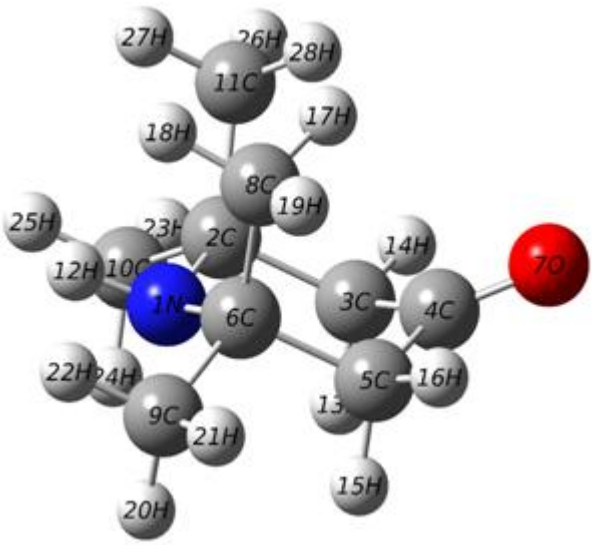


Figure 1: Optimized structure of TMP

Bond length	Value(Å)		
	a	b	c
N1-C2	1.48	1.47	1.51
N1-C6	1.48	1.47	1.51
N1-H12	1.02	1.00	1.37
C2-C3	1.55	1.53	1.53
C2-C10	1.54	1.54	1.54
C2-C11	1.55	1.53	1.53
C3-C4	1.52	1.51	1.53
C3-H13	1.10	1.08	0.99
C3-H14	1.09	1.09	0.99
C4-C5	1.52	1.51	1.54
C4-O7	1.21	1.19	-
C5-C6	1.55	1.54	1.53
C5-H15	1.10	1.09	0.99
C5-H16	1.09	1.08	0.99
C6-C8	1.55	1.54	1.54
C6-C9	1.54	1.53	1.53
C8-H17	1.09	1.09	0.98
C8-H18	1.09	1.08	0.98
C8-H19	1.09	1.09	0.98
C9-H20	1.09	1.09	0.98
C9-H21	1.09	1.09	0.98
C9-H22	1.10	1.09	0.98
C10-H23	1.09	1.09	0.98
C10-H24	1.09	1.09	0.98
C10-H25	1.10	1.09	0.98
C11-H26	1.09	1.09	0.98
C11-H27	1.09	1.09	0.98
C11-H28	1.09	1.08	0.98
Bond angle	**Value(°)**		
	a	b	c
C2-N1-C6	122.4	122.4	119.6
C2-N1-H12	110.3	110.1	117.7
C6-N1-H12	110.3	111.1	112.3
N1-C2-C3	107.8	109.4	108.6
N1-C2-C10	106.4	112.1	110.1
N1-C2-C11	115.3	107.7	110.8
C3-C2-C10	109.3	110.1	105.5
C3-C2-C11	109.7	109.1	111.2
C10-C2-C11	108.2	108.4	106.5
C2-C3-C4	112.0	113.9	113.1
C2-C3-C13	108.3	111.1	109.0
C2-C3-C14	111.1	109.6	109.0
C4-C3-H13	107.4	108.4	109.0
C4-C3-H14	109.3	106.6	109.0
C13-C3-H14	108.6	107.0	107.8
C3-C4-C5	114.0	116.2	109.8
C3-C4-O7	123.0	121.9	109.5
C5-C4-O7	123.0	121.9	109.5
C4-C5-C6	112.0	113.6	109.5
C4-C5-C15	107.4	106.5	109.5
C4-C5-H16	109.3	108.3	109.5
C6-C5-H15	108.3	110.1	109.5
C6-C6-H16	111.1	111.3	109.5
H15-C5-H16	108.6	106.8	109.5
N1-C6-C5	107.8	112.0	109.5
N1-C6-C8	115.3	109.2	109.5
N1-C6-C9	106.4	108.3	109.5
C5-C6-C8	109.7	109.6	109.5
C6-C8-H17	112.8	111.9	109.5
H20-C9-H21	109.0	108.1	109.5
H20-C9-H22	108.2	108.4	109.5
C2-C10-H23	110.9	110.9	109.5
C2-C10-H25	110.6	110.2	109.5
H23-C10-H24	109.0	107.7	109.5

Licensed Under Creative Commons Attribution CC BY

C2-C11-H26	110.2	111.3	109.5
C2-C11-H27	110.4	110.5	109.5
C2-C11-H28	112.8	110.4	109.5
H26-C11-H27	107.8	107.9	109.5
H26-C11-H28	107.2	108.9	109.5
H27-C11-H28	108.2	107.9	109.5

Dihedral Angle	Value(°)	
	a	b
C6-N1-C2-C3	52.224	-30.369
C6-N1-C2-C10	169.399	92.015
C6-N1-C2-C11	-70.625	-148.83
H12-N1-C2-C3	-175.460	-163.73
H12-N1-C2-C10	-58.284	-41.347
H12-N1-C2-C11	61.691	77.805
C2-N1-C6-C5	-52.221	-18.872
C2-N1-C6-C8	70.629	102.771
C2-N1-C6-C9	-169.399	-139.26
H12-N1-C6-C9	175.462	114.090
H12-N1-C6-C8	-61.689	-124.27
H12-N1-C6-C9	58.284	-6.297
N1-C2-C3-C4	-48.340	53.243
N1-C2-C3-H13	69.899	175.980
N1-C2-C3-H14	-170.893	-66.070
C10-C2-C3-C4	-163.634	-70.371
C10-C2-C3-H13	-45.395	52.367
C10- C2-C3-H14	73.813	170.317
C11- C2-C3-C4	77.905	170.797
C11- C2-C3-H13	-163.856	-66.465
C11- C2-C3-H14	-44.648	51.485
N1-C2-C10-H23	-175.659	176.109
N1-C2-C10-H24	-54.706	-63.115
N1-C2-C10-H25	65.057	57.021
C3-C2-C10-H23	-59.528	-61.895
C3-C2-C10-H24	61.425	58.881
C3-C2-C10-H25	-178.812	179.017
C11-C2-C10-H23	59.853	57.383
N1-C2-C11-H26	-169.653	179.905
C2-C3-C4-C5	53.489	-26.032
C2-C3-C4-O7	-126.577	153.927
H13-C3-C4-O7	114.682	29.728
H14-C3-C4-O7	-3.035	-85.088
C3-C4-C5-C6	-53.484	-24.563
O7-C4-C5-C6	126.581	155.478
O7-C4-C5-H15	-114.674	-83.224
O7-C4-C5-H16	3.042	31.252
C4-C5-C6-N1	48.332	47.252
C4-C5-C6-C8	-77.917	-74.164
C4-C5-C6-C9	163.623	167.170
N1-C6-C8-H19	169.619	176.752
C5-C6-C8-H17	51.273	60.267
C9-C6-C8-H19	50.608	58.867
N1-C6-C9-H20	54.696	62.390
N1-C6-C9-H21	175.648	-177.41
N1-C6-C9-H22	-65.068	-57.876
C5-C6-C9-H20	-61.437	-59.747
C8-C6-C9-H22	59.422	60.591

Generally, the C-N-C bond angles are slightly longer and shorter than the C-C-C or N-C-C bond angles [14]. Gundersen and Rankin reported the C-N-C (110.7^0), C-C-C (109.6^0) and N-C-C (110.5^0) bond angles by using electron diffraction technique [15]. In the present study, the bond angles of C-N-C (122.38^0), C-C-C (109.66^0) and N-C-C (107.7^0) by B3LYP method are depicted, in Table 1. The C-N bond lengths are predicted to be slightly shorter than the C-C bond lengths. Gundersen and Rankin [16] reported N-C (1.469 Å) and C-C (1.530 Å) by using electron diffraction technique. In TMP, the calculated bond length N-C (1.475 Å) and C-C (1.55 Å) by B3LYP/6-311++G (d, p) method have been noticed that the DFT calculations are consistent with the results of electron diffraction data [17]. The TMP exhibits the chair conformation with computed values of dihedral angles C6-C5-C4-C3, C5-C4-C3-C2, C4-C3-C2-N1, C4-C3-C2-N1, C4-C5-C6-N1, and C2-N1 –C6-C5 are –53.48^0, 53.48^0, - 48.34^0, 48.33^0, 52.22^0 and -52.22^0 respectively. It can be concluded that the chair form arises due to the van der Waals repulsion between the hydrogen atoms belonging to neighbouring carbon atoms.

HOMO−LUMO energy gap and related properties

HOMO−LUMO energy gap is used as a quantum chemical descriptor in establishing correlations in various chemical and biochemical systems [18]. The energy of the LUMO is directly related to the electron affinity and characterizes the susceptibility of the molecule towards attack by nucleophiles [19]. An electron affinity (EA) refers to the capability of a legend to accept precisely one electron from a donor. However, to influence the interacting systems, covalent or hydrogen bonding may take place which can result in a partial charge transfer [20].

A current approximation is to use Koopman's theorem to express these quantities in terms of the frontier one electron energy levels HOMO and LUMO [21-24]. The energy of the HOMO is directly related to the ionization potential (IP) and characteries the susceptibility of the molecules towards attack by electrophiles. Hard nucleophiles have a low HOMO energy while hard electrophiles have a high LUMO energy [25]. The operational definition of LUMO and HOMO in the context of DFT can be written as,

EA = −ξ LUMO

IP = −ξ HOMO

Where HOMO and LUMO correspond to the Kohn-Shan [26] one electron eigen values associated to the frontier molecular orbital HOMO and LUMO respectively. IP and EA refer to ionization potential and electron affinity of the system, respectively. The HOMO-LUMO energy gap for TMP was calculated at the B3LYP/6-311++ G(d,p) level is given in Table 2 and the visual comparison is shown in Fig. 2.

Table 2: Quantum chemical parameter of TMP

Chemical parameter	*Values*
Homo (eV)	-0.2041
Lumo (eV)	-0.0401
Ionization potential(I) (eV)	0.2041
Electron affinity(A) (eV)	0.0401
Global hardness(η) (eV)	0.0820
Global softness (S) (eV)	12.1921
Chemical potential(μ) (eV)	-0.1221
Electrophilicity (ω) (eV)	0.0908
Electro negativity(χ) (eV)	0.1221

Density functional theory (DFT) is possible to define and justify concepts of chemical reactivity such as the electronic chemical potential (μ), the absolute hardness (η), and the global electrophilicity (ω). The chemical potential μ of the

Licensed Under Creative Commons Attribution CC BY

electrons (the negative of the electronegativity (χ) is given by,

$$M = \left(\frac{\partial E}{\partial N}\right)_{v(r)}$$

$$\mu = -\frac{1}{2}(I + A)$$

And it has the same value everywhere. In a finite-difference approximation:

$$\chi = -\mu = \frac{1}{2}(I + A)$$

Where, I and A are the ionization potential and electron affinity. The change of μ with the number of electrons was defined by Parr and Pearson as a measure for the "absolute hardness" as

$$\eta = \left(\frac{\partial \mu}{\partial N}\right)_{v(r)} = \left(\frac{\partial^2 E}{\partial N^2}\right)_{v(r)}$$

The corresponding finite-difference formula is $\eta = \frac{1}{2}(I + A)$. The softness ($\sigma$) is reciprocal of the hardness (η). The electrophilicity index can be estimated by the equation [27]

$$\omega = \frac{\mu^2}{2\eta}$$

All the calculated values of quantum chemical parameters of TMP molecules in gas phase at DFT/B3LYP method with 6-311++G(d,p) basis set are presented in Table 2.

Hyperpolarisability

Organic non-linear materials have attracted a keen interest in recent year owing to their potential applications in various photonic technologies. Significant effects have focused on studying the electronic and structural properties of donor–acceptor substituted p-conjugated organic compounds with large molecular non-linear optical (NLO) response (β, first-order hyperpolarizability). Two factors are attributed to NLO properties of such compounds in an electric field: the altered ground state charge distribution by the donor and acceptor moieties and the enhanced- π -electronic charge redistribution through the π-conjugation. The first hyperpolarizability β is associated with the intramolecular charge transfer (ICT), resulting from the electron cloud movement through the π conjugated framework from electron donor to acceptor groups. The electron cloud is capable of interacting with an external electric field and thereby altering the dipole moment and the first hyperpolarizability.

The first hyperpolarizability (β) of this molecular system and related properties (β, α, Δα) of TMP are calculated and this is based on the finite field approach. In the presence of an applied electric field, the energy of a system is a function of the electric field. First hyperpolarizability is a third rank tensor that can be described by a 3x3x3 matrix. The 27 components of the 3D matrix can be reduced into 10 components due to the Kleinman symmetry. It can be given in the lower tetrahedral format. It is obvious that the lower part of the 3x3x3 matrices is a tetrahedral. The components of β are determined as the coefficients in the taylor series as the expansion of the energy in the external electric field where the external electric field is weak and homogeneous, this expansion becomes,

$$E = E^0 - \mu_\alpha F_\alpha - 1/2\alpha_{\alpha\beta}F_\alpha F_\beta - 1/6\beta_{\alpha\beta\gamma}F_\alpha F_\beta F_\gamma + \ldots\ldots$$

Where E^0 is the energy of the unperturbed molecule, F_α is the field at the original, μ_α, $\alpha_{\alpha\beta}$, $\beta_{\alpha\beta\gamma}$ are the components of the dipole moment, polarizability and the first hyperpolarizability respectively.

The title compound is fully optimised at B3LYP/6-311++G(d,p) method in the Gaussian 09W program. The tensor component of the static first hyperpolarisabilities, β, was analytically calculated by using the same method as mentioned above. From the computed tensorial component β, β^{vec} is calculated for the title compound by taking into account the kleinman symmetry relations and the squared norm of the Cartesian expression for the β tensor [28]. The relevant expression used for the calculations are shown below:

The total static dipole moment

$$\mu = (\mu_x^2 + \mu_y^2 + \mu_z^2)^{\frac{1}{2}}$$

The average hyperpolarizability

$$\beta = \sqrt{\left(\beta_x^{\,2} + \beta_y^{\,2} + \beta_z^{\,2}\right)}$$

Where, $\beta_x = \beta_{xxx} + \beta_{xyy} + \beta_{xzz}$,

$\beta_y = \beta_{yyy} + \beta_{xxy} + \beta_{yzz}$, $\beta_z = \beta_{zzz} + \beta_{xxz} + \beta_{yyz}$.

The isotropic polarizability

$$\alpha = \frac{\alpha_{xx} + \alpha_{yy} + \alpha_{zz}}{3}$$

The polarizability anisotropy invariant

$$\Delta\alpha = 2^{-1/2}[(\alpha_{xx} - \alpha_{yy})^2 + (\alpha_{yy} - \alpha_{zz})^2 + (\alpha_{zz} - \alpha_{xx})^2 + 6\alpha_{xx}^2]^{1/2}$$

Table 3: Theoretical first hyperpolarizability (α) along with theoretical dipolemoment (μ) of TMP using DFT/6-311++G(d,p) method.

Parameters	*Values*
Mean polarisability (α)	-3.2868×10^{-23} esu
Anisotropy of polarisability (Δα)	3.3567×10^{-5} esu
Dipole moment (μ)	3.8581D
First hyperpolarisability (β)	3.0035×10^{-31} esu
Vector-first hyperpolarisability (β_{vec})	0.50059×10^{-30} esu
μ x β	1.9313×10^{-30} esu

β^{vec} is the vector component along μ at zero frequency ,α is the mean polarizability and Δα is the anisotropy of the polarizability. The values of the Polarizabilities α and the hyper polarizability β of Gaussian 09W output are reported in atomic units (a.u). The calculated values have been converted into electrostatic units (esu). For α, $1 a.u = 0.1482 \times 10^{-24}$esu and for β, $1 a.u = 8.6393 \times 10^{-33}$esu.

There is an intense current research in the area of molecular linear and non-linear optics, devoted to the search for efficient, stable, simple organic compounds exhibiting large hyperpolarizabilities [29-32]. Theoretically, calculated values of first hyperpolarizability, dipole-moment and μ x β are shown in table 3. Analysing β and β_{vec}, it can be shown that there is an additive combination of the off-diagonal β-vectors to the total β due substitution in benzene. Such kind of behaviour (large off- diagonal contribution) has high

Licensed Under Creative Commons Attribution CC BY

practical utility in the NLO material research [33]. The calculated first hyperpolarizability of TMP is 3.0035 x 10^{-31} esu, which is 2.6 times greater than that of urea (0.37289 x10^{-30} esu). The total dipole moment μ and the mean polarizability are 3.8581D and -3.2868x10^{-23} esu. The μxβ value shows that there is a significant increase in optical non-linearities of the title compound.

Natural Bond Orbital analysis

NBO method encompasses a suite of algorithms that enable fundamental bonding concepts to be extracted from DFT computation. NBO analysis originated as a technique for studying hybridisation and covalency effects in polyatomic wave functions based on local block eigen vectors of the one particle density matrix [34]. NBO analysis provides the most accurate possible "natural Lewis structure" picture of ϕ, because all orbital details are mathematically chosen to include the highest possible percentage of the electron density. A useful aspect of NBO method is that it gives information about interactions in both filled and virtual orbital spaces that could enhance analysis of intra and inter molecular interactions. The second-order fock matrix was carried out to evaluate the donor-acceptor interactions in the NBO analysis [35].

The natural bonding orbital calculation [36] was performed at B3LYP level in order to investigate the electronic structure of the optimized geometry corresponds to the formation of hydrogen bonds. The hyper conjugative interaction energy was deduced second-order perturbation approach [37].

$$E^{(2)}_{i-j*} = -2\frac{\langle \sigma_i | F | \sigma^*_j \sigma \rangle^2}{\varepsilon_j - \varepsilon_i} = -2\frac{F^2_{ij}}{\Delta E}$$

where q_i is the donor orbital occupancy, ε_j and ε_i are diagonal elements and F(i ,j) is the off-diagonal NBO Fock matrix element. NBO analysis has been performed on the molecule TMP to identify and explain the formation of the strong intra molecular bonding between amine and carbon. The corresponding results have been tabulated in table 4. The importance of the hyper conjugative interaction and electron density transfer (EDT) from lone electron pairs the Y atom to the X-H anti-bonding orbital in the X-H….Y system have been reported by Reed et al [38].

Table 4: Natural bond orbital analysis of TMP

Bond (A-B)	ED/ Energy a.u.	ED_A (%)	ED_B (%)	NBO	S(%)	P(%)
BD (N1−C2)	1.9795	60.65	39.35	0.7788($sp^{1.62}$) N+ 0.6273($sp^{3.08}$) C	38.14 24.46	61.82 75.43
BD (N1−C6)	1.9794	60.65	39.35	0.7788($sp^{1.62}$)N+ 0.6273($sp^{3.08}$) C	38.14 24.46	61.82 75.43
BD (N1−H12)	1.9780	69.37	30.63	0.8329($sp^{3.23}$)N+ 0.5535 ($sp^{0.00}$) H	23.64 99.95	76.31 00.05
BD (C2−C3)	1.9610	49.24	50.76	0.7017($sp^{2.45}$)C+ 0.7125($sp^{2.31}$) C	28.98 30.22	71.00 69.70
BD (C2−C10)	1.9665	51.35	48.65	0.7166($sp^{3.29}$)C+ 0.6975 ($sp^{2.51}$) C	23.28 28.51	76.68 71.46
BD (C2−C11)	1.9665	51.35	48.65	0.7166($sp^{3.29}$)C+ 0.6975 ($sp^{2.51}$) C	23.28 28.51	76.68 71.46
BD (C3−C4)	1.9763	52.14	47.86	0.7221($sp^{2.56}$)C+ 0.6918 ($sp^{1.76}$)C	28.03 36.26	71.86 63.73
BD (C4−C5)	1.9763	47.86	52.14	0.6918($sp^{1.76}$)C+ 0.7221 ($sp^{2.56}$) C	36.26 28.03	63.73 71.86
BD (C4−O7)	1.9906	34.18	64.82	0.5931($sp^{2.65}$)C+ 0.8051($sp^{1.51}$) C	27.32 39.72	72.51 60.18
BD (C4−O7)	1.9838	29.26	70.74	0.5409($sp^{1.00}$)C+ 0.8411 ($sp^{1.00}$) C	26.52 29.21	73.44 70.75
BD (C5−C6)	1.9610	50.76	49.24	0.7125($sp^{2.31}$)C+ 0.7017($sp^{2.45}$) C	30.22 28.98	69.70 71.00
LP(N1)	1.8472			($sp^{1.00}$)	0.00	100.0
LP(O7)	1.9800			($sp^{0.66}$)	60.34	39.65
LP(O7)	1.9320			($sp^{1.00}$)	0.05	99.95
BD (C4−O7)	1.9838	29.26	70.74	0.5409($sp^{1.00}$)C+ 0.8411 ($sp^{1.00}$) C	26.52 29.21	73.44 70.75
BD (C5−C6)	1.9610	50.76	49.24	0.7125($sp^{2.31}$)C+ 0.7017($sp^{2.45}$) C	30.22 28.98	69.70 71.00

Table 5: Selected second order perturbation energies E(2) (donor →acceptor) for TMP

Donor NBO(i)	Acceptor NBO(j)	E(2) kcal/mol	E(j)−E(i) a.u.	F(i,j) a.u.
BD(N1-C2)	BD*(N1-C6)	4.42	1.33	0.069
BD(N1-C6)	BD*(N1-C6)	4.42	1.33	0.069
BD(N1-H12)	BD*(C5−C6)	0.98	1.13	0.030
BD(C5-H15)	BD*(C4−O7)	7.90	0.51	0.058
BD(C5-H16)	BD*(C4−O7)	7.90	0.51	0.058
BD(C8-H17)	BD*(C6−C9)	3.40	0.88	0.049
BD(C8-H18)	BD*(C5−C6)	2.44	1.04	0.045
BD(C8-H19)	BD*(N1−C6)	3.21	1.03	0.052
BD(C9-H20)	BD*(C6−C8)	3.40	0.88	0.049
BD(C9-H21)	BD*(N1−C6)	3.21	1.03	0.052
BD(C10-H23)	BD*(N1−C2)	3.21	1.03	0.052
BD(C10-H24)	BD*(C2−C11)	3.40	0.88	0.049
BD(C11-H26)	BD*(N1−C2)	3.21	1.03	0.052
BD(C11-H28)	BD*(C2−C10)	3.40	0.88	0.049
LP(N1)	BD*(C2−C10)	9.17	0.60	0.068
LP(O7)	BD*(C3−C4)	12.48	0.81	0.090
LP(O7)	BD*(C5−C6)	12.48	0.81	0.090

[a] $E^{(2)}$ means energy of hyper conjugative interaction (stabilization energy).

[b] Energy difference between donor and acceptor i and j NBO orbitals.

[c] F(*i,j*) is the Fock matrix element between i and j NBO orbitals

The table 4 shows the calculated natural orbital occupancy (number of electron (or)"natural population" of the orbital). It is noted that the maximum occupancies 1.9795, 1.9794, 1.9780 are obtained for BD (N1-C2), BD (N1-C6), and BD (N1-H12) respectively and corresponding *sp* composition are also tabulated. Therefore, the results suggest that the N1-C2, N1-C6 and N1-H12 bond lengths of these compounds are essentially controlled by the *p* -character of these hybrids orbital's and also by the nature of the N1-C2, N1-C6 and N1-H12 bonds.

Delocalisation of the electron density between occupancies Lewis type (bond (or) lone pair) NBO orbital and formally unoccupied (anti-bond (or) Rydberg) non-Lewis NBO orbital corresponding to a stabilizing donor-acceptor interaction have been performed at B3LYP/6-311++G (d,p).

Licensed Under Creative Commons Attribution CC BY

The energy of these interactions can be estimated by the second order perturbation theory [39]. Table 5 list the calculated second-order interaction energies ($E^{(2)}$) between the donor-acceptor orbital in TMP. The most important interaction energies, related to the resonance in the benzene ring are electron donating from the LP(N1), LP(O7),LP(O7) to the anti-bonding acceptor BD*(C2-C10), BD*(C3-C4) and BD*(C5-C6) orbital.

The stabilization energy E(2) associated with the hyperconjugative interactions viz. LP(N1) → BD*(C2–C10), LP(O7) → BD*(C3–C4), LP(O7) → BD*(C5–C6), are obtained 9.17, 12.48, 12.48 kcal mol^{-1} respectively, as shown in Table 5. It is worth mentioning that, the differences in stabilization energies reported in Table 5 are reasonable. In view of the fact that, the accumulation of electron density in the antibonding orbital σ*(C–C) is not only transferred from the loan electron pair LP (N1) and LP(O7) but also from the entire molecule.

Vibrational Assignments

The molecular structure TEMP is shown in fig. 1. From the structural point of view the molecule is assumed to have C1 point group symmetry. The present molecule TEMPO consists of 31 atoms, so it has 87 normal vibrational modes. The observed FT-IR and FT-Raman spectra are shown in Figs. 3 and 4, respectively. The detailed vibrational assignments of fundamental modes of TEMP along with observed and calculated frequencies and normal mode descriptions have been reported in Table 6. It is convenient to discuss the vibrational spectra of TMP in terms of characteristic spectral region as describe below.

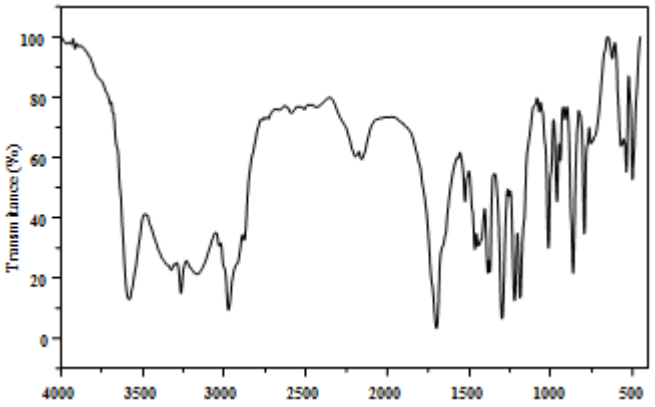


Figure 3: FT-IR spectrum of TEMP

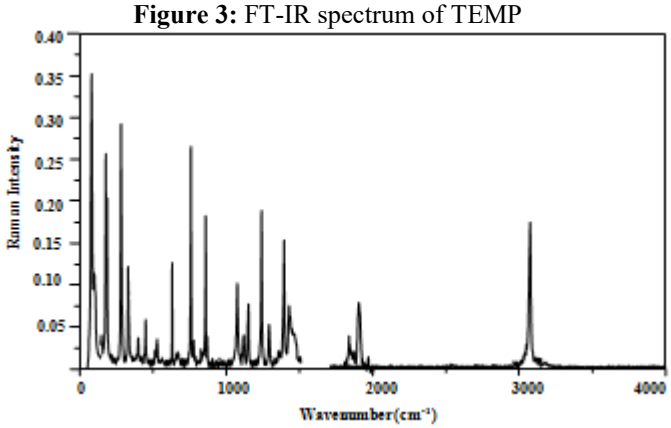


Figure 4: Raman spectrum of TEMP

Table 6: Vibrational assignments, infrared intensities, Raman activities and Raman intensity of TMP based on HF and B3LYP/6-311+G** method

Observed frequencies cm^{-1}		Calculated frequencies cm^{-1}				Reduced mass (amu)		Force constant ($mdyneA^{-1}$)		IR intensity $(km)mol^{-1}$		Raman activity A^0(amu)		Raman intensity $(km)mol^{-1}$		Assignments/ (%PED)
FTIR	FT−Raman	Unscaled		Scaled												
		a	b	a	b	a	b	a	b	a	b	a	b	a	b	
3321		3800	3522	3588	3326	1.08	1.07	9.15	7.85	2.77	0.13	49.22	82.79	6.40	0.40	νNH(100)
2972		3248	3129	3083	2970	1.10	1.10	6.84	6.32	21.13	22.42	94.25	39.24	20.86	0.27	νCH_{3as}(99)
		3244	3111	3080	2953	1.10	1.10	6.83	6.28	20.10	31.51	96.67	36.68	21.49	0.26	νCH_{3as}(98)
		3241	3109	3077	2951	1.10	1.10	6.81	6.27	61.15	35.47	38.56	177.18	8.60	1.26	νCH_{3as}(96)+νCH_{2as}(81)
		3239	3107	3075	2949	1.10	1.10	6.81	6.27	42.47	25.95	41.08	15.81	9.17	0.11	νCH_{3as}(97)+νCH_{2as}(82)
		3236	3104	3072	2947	1.10	1.10	6.78	6.25	96.68	5.23	88.75	34.14	19.88	0.24	νCH_{2as}(95)+ νCH_{3as}(78)
		3230	3103	3066	2946	1.10	1.10	6.76	6.23	12.46	9.38	41.60	41.28	9.37	0.30	νCH_{2as}(98)+ νCH_{3as}(81)
		3223	3087	3060	2930	1.10	1.10	6.73	6.18	19.25	61.38	46.16	183.51	10.47	1.34	νCH_{3as}(99)+ νCH_{2as}(80)
		3220	3085	3057	2929	1.10	1.10	6.73	6.17	58.16	38.16	93.77	30.46	21.32	0.22	νCH_{3as}(99)+νCH_{2as}(82)
		3218	3079	3055	2923	1.10	1.10	6.73	6.15	35.60	7.08	44.24	21.82	10.09	0.16	νCH_{3as}(91)
		3210	3078	3047	2922	1.10	1.10	6.69	6.14	1.15	0.12	10.65	15.70	2.45	0.12	νCH_{3as}(93)
		3187	3033	3025	2879	1.07	1.06	6.39	5.73	2.94	1.19	203.57	508.66	47.79	3.90	νCH_{3s}(97)+ν CH_{2s}(75)
		3182	3029	3021	2875	1.07	1.05	6.37	5.66	14.90	50.95	86.03	108.70	20.29	0.84	νCH_{3s}(95)+()+ν CH_{2s}(73)
		3165	3029	3005	2875	1.04	1.05	6.14	5.65	34.72	24.28	68.06	1.53	16.32	0.01	νCH_{2s}(98)+ν CH_{3s}(71)
		3162	3023	3002	2870	1.04	1.06	6.13	5.69	27.61	1.67	258.43	13.65	62.11	0.11	νCH_{2s}(93)+ν CH_{3s}(77)
		3156	3020	2996	2867	1.04	1.04	6.08	5.57	23.57	28.23	42.02	114.26	10.16	0.89	νCH_{3s}(94)
		3155	3019	2995	2866	1.04	1.04	6.09	5.57	25.09	10.80	2.20	7.80	0.53	0.06	νCH_{3s}(76)
		1980	1777	1880	1687	11.59	10.82	26.77	20.12	339.66	247.85	17.12	17.16	13.17	0.46	νCO(88)
		1658	1520	1574	1443	1.28	1.17	2.07	1.59	21.52	12.71	1.62	2.19	1.77	0.08	ρ CH3(79)+ρ CH_2(60)
1463		1627	1519	1569	1465	1.06	1.06	1.65	1.44	4.97	9.79	1.17	1.51	1.32	0.05	ρ CH3(78)
1444		1625	1506	1567	1452	1.06	1.05	1.65	1.41	6.00	0.92	1.84	9.49	2.08	0.35	ρ CH3(88)+ρ CH_2(24)
1434	1430	1621	1501	1563	1447	1.06	1.05	1.64	1.40	1.93	7.51	12.55	2.18	14.25	0.08	ρ CH3(85)+ρ CH_2(21)
1422	1430	1612	1491	1554	1438	1.08	1.05	1.66	1.38	11.84	8.04	3.97	1.55	4.55	0.06	ρ CH3(79)+ρ CH_2(25)
1422		1609	1488	1552	1435	1.06	1.05	1.61	1.37	11.52	7.72	0.77	8.33	0.88	0.31	ρ CH3(75)+ρ CH_2(69)

Licensed Under Creative Commons Attribution CC BY

	1396	1604	1484	1499	1387	1.06	1.05	1.60	1.36	3.68	0.83	3.74	1.25	4.32	0.05	ρ CH3(78)+ρ CH_2(65)
		1601	1477	1496	1380	1.06	1.05	1.59	1.35	4.46	0.13	9.65	5.58	11.21	0.21	ρ CH3(95)
		1598	1471	1493	1374	1.05	1.09	1.59	1.39	2.22	5.70	10.23	0.54	11.92	0.02	CH_{2sciss}(60)
1396		1586	1471	1482	1374	1.10	1.15	1.63	1.46	2.98	12.52	4.75	15.88	5.61	0.60	ρ CH3(+ρ CH2(67)
		1578	1457	1474	1361	1.09	1.11	1.59	1.38	17.93	16.96	2.18	4.00	2.59	0.16	CH_{2sciss}(60)
1383		1545	1423	1490	1372	1.25	1.22	1.76	1.45	18.53	8.37	0.66	0.30	0.82	0.01	sbCH3(96)
		1544	1414	1489	1364	1.25	1.23	1.76	1.46	11.00	17.44	1.07	0.71	1.32	0.03	sb CH3(69)
		1527	1401	1472	1351	1.30	1.24	1.78	1.44	18.04	22.94	0.23	0.11	0.29	0.00	sb CH3(66)
		1526	1396	1472	1346	1.30	1.24	1.79	1.42	4.52	1.94	0.35	0.12	0.44	0.00	sbCH3(65)
	1293	1480	1332	1427	1284	2.05	1.74	2.64	1.82	1.62	19.32	3.51	2.38	4.69	0.11	CH2(62)wag
1254		1460	1312	1408	1265	1.88	2.21	2.36	2.24	17.67	77.13	1.33	3.00	1.82	0.14	CH2(61) wag
	1242	1409	1289	1359	1243	2.14	2.14	2.50	2.10	14.83	24.22	6.10	11.73	8.88	0.56	t CH2(60)
1220		1361	1270	1312	1225	1.79	1.52	2.05	1.44	39.85	3.12	2.07	0.95	3.06	0.05	t CH2(64)
1186		1376	1269	1284	1184	3.43	1.80	3.83	1.71	104.65	11.79	4.31	10.15	6.52	0.50	t CCNH(62)
1186		1397	1246	1332	1188	1.75	2.58	1.92	2.36	2.04	75.41	4.67	2.49	7.20	0.13	δCH3(71)+δ CH_2(69)
1186		1317	1210	1255	1153	2.22	2.73	2.27	2.35	22.64	5.86	1.89	2.52	3.08	0.13	δ CH3(73)+δ CH_2(65)
	1152	1302	1185	1257	1144	2.39	2.13	2.39	1.76	6.56	4.88	3.35	0.68	5.57	0.04	δ CH3(77)+δ CH_2(69)
1118		1282	1167	1238	1127	2.34	1.83	2.26	1.47	8.92	10.39	4.13	10.07	7.05	0.56	δ CH3(71)+δ CH_2(65)
	1076	1255	1167	1166	1084	2.33	3.11	2.16	2.49	11.92	6.91	1.28	5.80	2.27	0.32	δ CH3(79)+δ CH_2(65)
		1210	1078	1124	1001	1.37	1.46	1.18	1.00	0.85	0.02	8.57	2.94	16.05	0.19	CH2(66)rock
1000		1140	1046	1093	1003	1.85	1.57	1.42	1.01	13.24	0.29	1.77	1.29	3.65	0.09	CH2(63) rock
		1120	1030	1074	988	1.43	1.85	1.06	1.16	0.59	6.50	2.59	0.95	5.48	0.06	δ CH3(67)+δ CH_2(65)
961		1101	1011	1047	961	1.29	1.37	0.92	0.83	0.50	0.25	1.88	1.77	4.08	0.12	νCN(89)
940		1062	1007	1010	957	1.74	1.55	1.15	0.92	0.47	3.24	7.00	1.90	16.08	0.13	δ CH3(65)+δ CH_2(65)
		1045	942	994	896	1.68	1.43	1.08	0.75	3.01	0.87	2.59	2.82	6.12	0.22	δ CH3(91)+δ CH_2(65)
		1012	931	962	885	1.64	1.76	0.99	0.90	0.10	0.00	4.38	5.90	10.83	0.47	b CCO(77)
862	860	1009	928	937	862	1.59	1.67	0.95	0.85	1.10	0.63	5.01	4.64	12.46	0.37	RING(50)+νCCC(35)
		1001	917	930	852	1.52	1.81	0.90	0.90	0.04	0.09	7.59	3.27	19.08	0.26	νCC(95)
		982	900	912	836	1.91	2.18	1.09	1.04	0.16	0.34	0.37	10.62	0.95	0.88	νCC(92)
		968	874	899	812	2.40	3.84	1.33	1.73	1.96	5.36	3.80	4.44	10.06	0.39	νCC(74)
		874	866	812	804	2.54	1.98	1.15	0.88	1.49	4.74	3.32	0.14	10.23	0.01	νCC(85)
793		861	814	839	794	3.22	2.51	1.41	0.98	0.56	8.46	0.05	4.86	0.16	0.47	νCC(51)
753	759	813	767	793	748	2.29	2.78	0.89	0.96	2.17	0.21	11.60	0.02	39.75	0.00	νCC(49)
	631	674	646	657	630	2.29	2.34	0.61	0.58	58.27	65.44	3.65	2.89	16.40	0.39	RING (48)
		603	609	588	594	3.03	3.68	0.65	0.80	1.70	13.15	15.73	19.35	83.02	2.84	νCC(57)
		596	552	581	538	2.41	2.74	0.50	0.49	7.27	0.64	3.36	7.61	17.99	1.29	RING(46)
		576	537	562	524	2.88	3.06	0.56	0.52	15.44	10.59	1.15	0.62	6.48	1.52	b CCC(41)
462		497	472	485	460	3.88	3.09	0.57	0.41	2.31	2.06	1.80	1.15	12.55	2.04	νCC(47)
450	450	473	471	461	459	2.73	1.58	0.36	0.21	2.01	22.91	0.74	0.70	5.53	2.26	RING (42)
		463	453	451	442	2.26	2.12	0.29	0.26	10.41	0.17	0.17	0.04	1.28	2.62	b CCC(44)
		438	398	427	388	2.35	2.27	0.27	0.21	5.72	2.24	0.34	0.55	2.82	3.44	b CCC(46)
330	330	414	369	404	335	2.23	2.89	0.23	0.23	7.76	0.70	1.15	0.69	10.49	4.17	b CCC(44)
		381	359	371	350	2.14	3.22	0.18	0.25	0.49	3.16	0.32	1.76	3.34	4.67	b CCC(55)
330		365	355	356	346	2.36	2.50	0.19	0.19	0.71	0.89	0.78	1.59	8.57	5.08	b CCN(47)+γCCCO(28)
		332	312	324	304	1.70	2.28	0.11	0.13	2.13	0.98	0.51	1.40	6.55	6.61	b CCC(43)
	282	320	299	297	278	1.78	1.44	0.11	0.08	0.26	1.61	0.82	0.48	11.11	7.46	b CNC39()
		311	269	289	250	1.57	1.55	0.09	0.07	0.82	0.08	0.97	0.81	13.77	9.36	RING(33)
		286	254	266	236	1.39	1.36	0.07	0.05	1.22	0.38	0.17	0.39	2.73	10.83	t CH3(81)
		262	247	243	229	1.40	1.40	0.06	0.05	0.42	0.44	0.24	0.18	4.44	11.88	t CH3(79)
		249	236	231	219	1.11	1.26	0.04	0.04	0.29	0.15	0.04	0.29	0.87	13.43	t CH3(88)
	186	238	203	221	189	1.17	1.06	0.04	0.03	0.57	0.42	0.07	0.01	1.46	18.00	t CH3(68)
		157	152	146	141	2.66	2.58	0.04	0.04	0.07	0.11	0.05	0.25	2.19	30.72	t CCNC(30)
		82	86	76	80	3.94	5.29	0.02	0.02	4.48	4.93	0.61	0.82	85.47	88.48	RING(38)
82	82	61	82	61	82	3.06	2.80	0.01	0.01	3.48	0.42	0.41	0.24	100.00	100.00	t HCCO(56)

[a] Calculated by B3LYP/6-311+G**
[b] Calculated by HF/6-311++G**

Intensities: w-weak, vw-very weak, s-strong, vs-very strong. ν-stretching, ss-symmetric stretching, ass-asymmetric stretching, sd-in-plane bending, ad-out-of-plane bending, sciss.-scissoring, wag.-wagging, rock.-rocking, ipd-in-plane bending, opd-out-of-plane bending, ipr.-in-plane rocking, opr.-out-of-plane rocking, twist.-twisting, δ_{ring} - ring in-plane-bending, γ_{ring} - ring out-of-plane-bending

Methyl and Methylene Vibration

The asymmetric stretching for the CH_2 and CH_3 has magnitude higher than the symmetric stretching [40, 41]. For

Licensed Under Creative Commons Attribution CC BY

the assignments of CH_3 group frequencies, nine fundamentals can be associated to each CH_3 group [42]. The C–H stretching in CH_3 occurs at lower frequencies than those of aromatic ring (3100–3000 cm^{-1}). For TMP, the weak intensity peak at 2972 cm^{-1} in FT-IR spectra is assigned to CH_3 asymmetric stretching vibration, whereas CH_3 symmetric stretching is absent in both spectra. Moreover, in this molecule, the asymmetric CH_2 stretch calculated with B3LYP after scaling down gives the value of 2947 cm^{-1} and 2946 cm^{-1}, while the symmetric stretch was calculated at 2875 cm^{-1} and 2870 cm^{-1}.

According to the calculated TED, our calculation shows that there are pure vibrations which are in agreement with the literature [43]. The deformation of CH_3 group is usually observed in the range 1450–1400 cm^{-1} for methyl substituted aromatic rings [44, 45]. The weak peaks at 1463, 1444, 1434, 1422 cm^{-1} and 1186, 1118 cm^{-1} are assigned to scissoring and rocking vibrations of CH_3. The strong peak at 1297 cm^{-1} and very weak peak at 1293 cm^{-1} of FT-IR and FT-Raman are assigned to wagging vibration of CH_2.

In accordance with assignment column in Table 6, it is clear that most of the wagging modes of CH_2., are observed for FT-IR at 1254 cm^{-1} as a medium strong band and FT-Raman at 1293, 1242 cm^{-1} as very weak band. The CH_2-torsion is observed at 1220 cm^{-1} in FT-IR spectrum of TMP. In this study, the C - CH_3 out-of-plane bending (torsion) vibration mode, were calculated at 236, 229, 219 cm^{-1} for B3LYP method and 266, 243, 231, 186 cm^{-1} for DFT method. All other modes are mixed modes and shown in the TED column of Table 6.

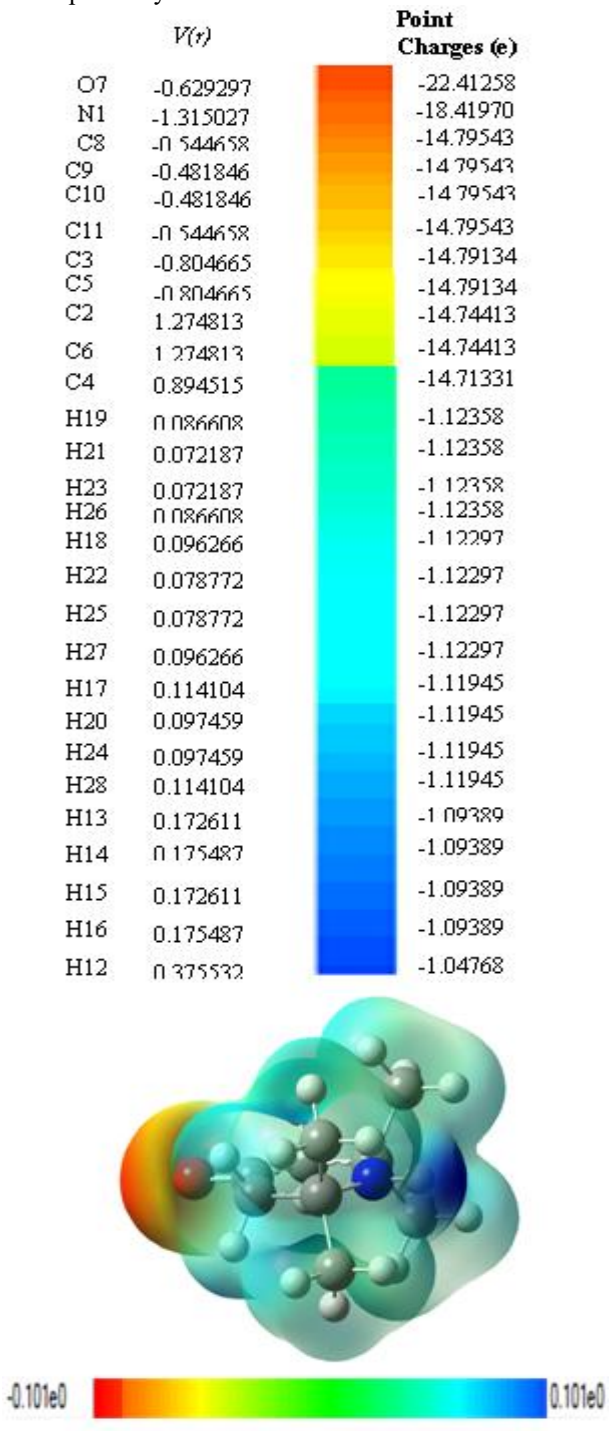
CO Vibration

Carbonyl group vibrations give rise to characteristic bands in vibrational spectra and for this reason such bands have been a subject of extensive studies [46 - 48]. The C=O stretching frequency appears strongly in the FT-IR spectrum in the range 1850-1600 cm^{-1}. The absorptions are sensitive for both carbon and oxygen atoms of the carbonyl group. Both have the same amplitudes while it vibrates. Normally, carbonyl group vibrations occur in the region 1780−1680 cm^{-1} [49]. In the present study, the C=O stretching vibrations is assigned at 1700 cm^{-1} in FT-IR. According to the literature, the C=O vibration is pushed to the lower region by the influence of amine group vibration, because of the proximity.

Ring Vibration

The ring stretching vibrations in each compound readily assigned in the range 1590−1000 cm^{-1} [50, 51]. The ring mode manifests as medium strong in IR at 862 cm^{-1} and very weak in Raman at 860 cm^{-1}.The FT-IR and FT-Raman bands at 753, 793cm^{-1} and 759 cm^{-1}, 450 cm^{-1} are assigned to ring stretching vibrations. All the stretching modes are expected to appear in the expected range. As expected, all the bands are observed with very weak and medium intensities. It shows good agreement between theoretical and experimental CC stretching vibrations. The identification of CN stretching frequency is a rather, difficulty task, since the mixing of vibration is possible in this region. The CN frequency vibrations usually lie in the region 1400-1200 cm^{-1} which is observed strongly for FT-IR at 961cm^{-1} as a very weak band.

The CCC bending vibrations always occur below the region 600 cm^{-1} [52]. The weak band of FT-IR is assigned to CC in plane bending vibrations at 498 cm^{-1}. The calculated CC in plane bending vibrations assigned at 442, 388, 360 cm^{-1} are assigned in B3LYP method and 427, 427, 404 cm^{-1} in HF method. The NH stretching vibrations generally appear in the range 3500-3300 cm^{-1} [53, 54]. The observed weak band in IR at 3321cm^{-1} corresponds to NH stretching mode. The bending vibration is assigned to FT-Raman at 330 cm^{-1} as a strong band. The ring vibrations are assigned to FT-IR and FT-Raman at 622 cm^{-1},536 cm^{-1} as a weak bands and 631 cm^{-1},450 cm^{-1}, 82 cm^{-1} as a weak, very weak and very strong band respectively.



Licensed Under Creative Commons Attribution CC BY

4. Molecular Electrostatic Potential

Molecular Electrostatic potential (MEP) generally presents in the space around the molecule. The charge distribution is very useful in understanding the sites of electrophilic attacks and nucleophilic reaction for the study of biological recognition process [55] and hydrogen bonding interactions [56]. In order to predict the molecular interactive sites, the MEP for our title molecule TMP is calculated by B3LYP/6-311++G (d,p) method as shown in Fig. 5. In MEP map, there are several possible sites for electrophilic attacks over oxygen atoms. The different values of the electrostatic potential at the surface are represented by different colours; red represents regions of most negative electrostatic potential, blue represents regions of most positive electrostatic potential and green represents regions of zero potential. The maximum negative electrostatic potential is noted over N1, C3, O7 atoms. For the possible nucleophilic reaction, the maximum positive region is on methyl and ethylene group and partially over the aromatic H atoms. The results of the MEP shows that negative potential are presented at electronegative carbon atoms, whereas positive potential are present at hydrogen atoms.

Solvent effect on the UV/vis spectrum

The chemical structure of TMP is composed of a conjugated system of double bonds and aromatic ring. Natural bond orbital analysis indicates that molecular orbitals are mainly composed of π atomic orbital, so above electronic transitions are mainly derived from the contribution of bands π-π* where occupied orbitals have π character while unoccupied ones have a π* character. UV-Vis absorption spectrum of the sample in gas and solvents like DMSO, ethanol and acetone is shown in fig. 6. There are three wavelengths for all the solvents. In TMP molecule, except the gas phase all other solvents have larger wavelength and the larger energy gap value. Thereby, absorption induces a red shift of the compound going from gas phase. Whatever the environment, the first peak is around 339 nm for gas and around 378 nm for other solvents, while the second peak, the most intense peak is around 295nm for gas phase and 291 nm for other solvents. Moreover, Table 7 shows the corresponding information could be retrieved through the higher oscillator strengths observed in solvents than in gas phase.

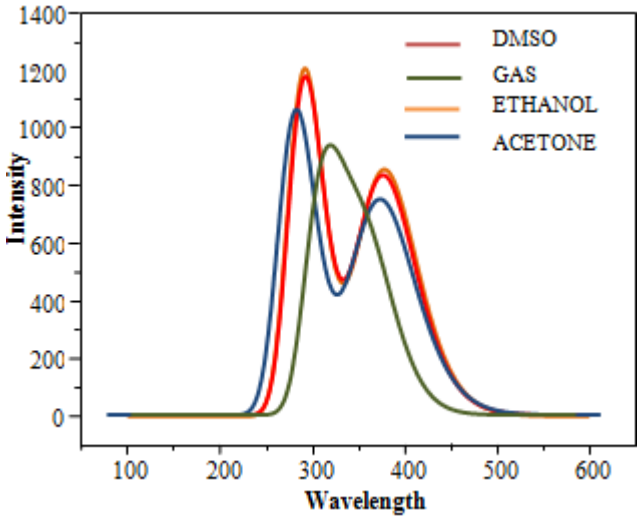


Figure 6: UV-vis spectrum of TMP

Thus, the solvent cases the absorption with the maximum oscillator strength of DMSO. Gauss-Sum 2.2 program [57] was used to calculate group contributions to the molecular orbitals (HOMO and LUMO) and prepare the density of states (DOS) spectrum in Fig. 6. The DOS spectra were created by convoluting the molecular orbital information with GAUSSIAN

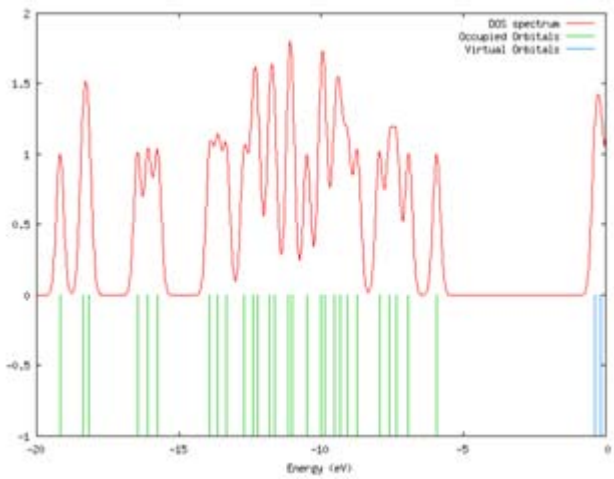


Table 7: Computed excitation energies, oscillator strength and electronic transition configuration of TMP.

Solvents	B3LYP λ(nm)	Energy (eV)	Oscillator Strength (*f*)	Major contribution ≥ (10%)
Gas	339.49	3.6521	0.0141	H →L(100)
	332.06	3.7338	0.0001	H-1→L (98%)
	295.36	4.1978	0.0208	H→L+1 (97%)
Water	378.29	3.2775	0.0204	H→L (100%)
	311.82	3.9762	0.0001	H-1→L (99%)
	291.64	4.2513	0.0290	H→L+1 (97%)
Dmso	377.92	3.2807	0.0211	H→L (100%)
	312.24	3.9708	0.0001	H-1→L (99%)
	291.62	4.2515	0.0298	H→L+1 (97%)
Ethanol	376.56	3.2925	0.0205	H→L (100%)
	312.92	3.9622	0.0001	H-1→L (99%)
	291.54	4.2528	0.0291	H→L+1 (97%)
Acetone	376.01	3.2974	0.0205	H→L (100%)
	313.22	3.9584	0.0001	H-1→L (99%)
	291.54	4.2527	0.0290	H→L+1 (97%)

Licensed Under Creative Commons Attribution CC BY

curves of unit height. The green and blue lines in the DOS spectrum indicate the HOMO and LUMO levels.

5. Conclusion

The optimized geometric parameters of the title compound were interpreted and compared with the earlier reported experimental values of a similar compound. The lowering of HOMO and LUMO energy gap clearly explains the charge transfer interactions taking place within the molecule. The calculated first order hyperpolarisability of TMP is $0.50059x10^{-30}$ e.s.u which is 1.34 times greater than that of urea. The shifting of the methyl stretching wavenumber is due to the hyperconjugative interaction between the σ(C-H) —›σ*(C_4-O_7)bond and is confirmed by NBO analysis. The FT-IR and FT-RAMAN spectra of the compound were recorded and the vibrational modes were assigned with the aid of the experimental and the computed vibrational wave numbers. The results of the molecular electrostatic potential shown that the negative potential are presented at the electronegative carbon atoms whereas positive potential are presented at hydrogen atoms. Finally, it is worthy to mention that solvent induces a considerable red shift of the absorption maximum of the compound going from the gas phase.

6. Acknowledgement

This work was supported by the University Grants Commissions fund through research Grant no.: MRP-5124/14 (SERO/UGC).

References

[1] Microchemical Journal July 2011,vol98(2):204-206 doi:10.1016
[2] Mieczyslaw Makosza, Pure Appl.chem 2000.72(7);1399-1403
[3] Wikipedia .org
[4] J.Chem.pharm.Res., 2010 ,2(2);581-589.
[5] Cunico W,Claudia RB, Ferreira MG, capri LR, Soares M, 2007 ;48:6217-20
[6] M.J. Frisch et al., GAUSSIAN 09, Revision A.9, Gaussian, Inc., Pittsurgh, 2009.
[7] A.D. Becke, J.chem. phys.98 (1993)5648-5652.
[8] C.Lee, W.Yang, R.G.Parr,Phys. Rev. B 37 (1988) 785-789.
[9] T. Sundius, MOLVIB; A program for harmonic force field calculations, QCPE Program no. 604, J. Mol. Struct. 218 (1990) 321.
[10] T. Sundius, Vib. Spectrosc. 29 (2002) 89.
[11] G.Keresztury, S.Holly,J.Varga,G.Besenyei,A.Y.wang,J.During, Spectrocim. Acta 49A (1993) 2007-2026.
[12] G.Keresztury, J.M. Chalmers,P.R Griffith (Eds.), Raman spectroscopy: Theroy, Handbook of vibrational spectroscopy, vol. 1,John Wiley&sons Ltd., New York, 2002.
[13] S. K. Goswami, L. R. Hanton, C. J. McAdam, S. C. Moratti and J. Simpson, *ActaCryst.* (2011). E67, o3024-o3025]
[14] N. Akbay, Z. Seferoglu. E. Gok, J. Fluoresc. 19(2009) 1045-1051.
[15] N. B. Colthup, L.H. Daly, S.E. Wiberley, Introduction to Infrared and Raman Spectroscopy, Academic Press, New York, 1990.
[16] N.Francisco,V.Ricardo,J.Mol.Struct.(Theochem) 850 (2008) 127-134
[17] M.Karelson,V.S.Lobanov,Chem.Rev.96(1996)1027-1043,
[18] P.Thanikaivelan,V.Subramanian,V.RRahava,B.N.Unni, Chem.Phys.Lett.323 (2000)59-70
[19] R.Contreras,P.Fuentealba,M.Galvan,P.Perez,Chem.Phys .Lett.304(1999)405-413
[20] P.Fuentealba,R.Contreras,in:K.D.Sen(Ed.),Reviews of Modern Quantum chemistry,vol.II,world Scientific,Singapore,2002
[21] P.Fuentealba ,P.Perez,R.Contreras ,J.Chem.Phys.113(2000)2544-2551
[22] I.Fleming,Frontier orbitals and organic chemical reactions.John Wiley and sons,New York,1976
[23] C.Ravikumar ,I.Hubert Joe,Phys.Chem.Chem.Phys.12(2010)9452-9460
[24] W.Kohn, I.Shan,J.Phys .Rev.140(1965)1133-1138.
[25] B.C.,Smith,Infrared Spectral Interpretation,CRC Press,Boca Raton, FL., 1996.
[26] L.J. Bellamy, The Infrared spectra of compound molecules,Chapman and Hall London.1975.
[27] D. Sajan, J. Binoy, B. Pradeep, K. Venkatakrishnan, V. Kartha, I. Joe, V.Jayakumar, 2004.Spectrochim . Acta A 60: 173-180.
[28] D.A .Kleinman, Phys.Rev.126 (1962) 1977-1979
[29] U.Gubler,S.Concilio,C.Bosshard,I.Biaggio,P.Gunter,R. E.Martin,M.J.Edelman, J.Wytko, F.Diederich, Appl.Phys. Lett. 81 (2002) 2322-2324
[30] P.Acebad, S.Blaya, L.Carretero .J.Phys.B.Atom.Mol.Opt.Phys.36(2003)2445-2454.
[31] G. Maroulis ,Atoms, Compounds and clusters in Electric field ,Imperial college Press, London .2006
[32] J.L.Bredas,C.Adant.P.Tacxx,A.Persoons,B.M.Pierce ,Chem.Rev.94(1994)242-278.
[33] J.J .Wolf, F. Siegler,R. Matschiner , R .Wortmann ,Angew . Chem .Int .Ed .Eng .391 (2000) 436
[34] J.P. Foster, F. Weinhold A.Chem.Soc.102 (1980)7211-7218.
[35] M.Szafran A. Komasa, E.B.Adamska, .Mol. Struct-Theochem 827 (2007)101-107 .24. A.E. Reed, L.A Curtiss, F. Weinhold , Chem. Rev 88(1988) 899-926.
[36] E.D. Glendening, A.E, Reed, J.E. Carpender, F.W. Weinhold, NBO Version 3.1 TCI, University of Wisconsin, Madison, 1998.
[37] J. Chocholousova,V.Spirko, P.Hobza, Phys.Chem. Chem. Phys.6(1)(2004) 37-41.
[38] A.E. Reed, L.A Curtiss, F. Weinhold , Chem. Rev 88(1988) 899-926.
[39] Hubert Joe , I. Kostova, C. Ravikumar, M. Amalanthan, S.C. Pinzaru, J. Raman spectrosc.40(2009) 1033-1038.
[40] D. Lin-Vien, N.B. Colthup, W.G. Fateley, J.G. Grasselli, The Handbook of Infrared and Raman Characteristic Frequencies of Organic Molecules, Academic Press, Bostosn, MA, 1991.
[41] Altun, K. Gölcük, M. Kumru, J. Mol. Struct. (Theochem.) 625 (2003) 17–24.

Licensed Under Creative Commons Attribution CC BY

[42] P.S. Kalsi, Spectroscopy of Organic Compounds, Wiley Eastern Limited, New Delhi, 1993.
[43] .M. Karabacak, E. Sahin, M. Cinar, I. Erol, M. Kurt, J. Mol. Struct. 886 (2008) 148– 157.
[44] G. Socrates, Infrared and Raman Characteristic Frequencies, 3rd ed., John Wiley & Sons Ltd., Chichester, 2001.
[45] D.L. Vein, N.B. Colthup, W.G. Fateley, J.G. Grasselli, The Handbook of Infrared and Raman Characteristic Frequencies of Organic Molecules, Academic Press, San Diego, 1991.
[46] H.Ringertz,Acta. Crystallogr. B 27 (1971) 285.
[47] F.R.Dollish, W.G. Fateley, F.F.Bentley , characteristic Raman Frequencies of organic compounds , Joh wiley & Sons , New York , 1997.
[48] N.B.Colthup , L.H. Daly ,S.E. Wiberley , Introduction to Infrared and Raman Spectroscopy . Academic Press, New York, 1990.
[49] J.Mohan,Organic spectroscopy–Principle and Applications, Second ed.,norosa publishing House , New Delhi , 2000 pp 30-32 .
[50] G.Socrates , Infrared Characteristic Group frequencies , John Wiley and Sons , middlesser , 1980.
[51] K.Parimala , V.Balachandran .Spectrochim. Acta 81A(2011)711-723
[52] G.Gunasekaran , E.Sailatha ,Indian J.pure Appl.phys.47(2009) 259-264
[53] L.J.Bellamy, The infrared spectra of complex molecules, John Wiley and sons Inc.,New York ,1975.
[54] A.spir,M.Barthes , H.Kellwai , G.De Nunzio, Physicsa D 137 (2000) 392.
[55] P.B.Nagabalasubramanian,S.Periandy,S.Mohan,Spectro chim, Acta A 77(2010) 150-159.
[56] V.Krishnakumar, V.Balachandran, Spectrochim.Acta A 62 (2005) 918-925.
[57] N.M.O'Boyle,A.L.Tenderholt,K.M Langer,J.Comput.Chem.29(2008)839-845.

Licensed Under Creative Commons Attribution CC BY